THE JOURNAL OF PHYSICAL CHEMISTRY A
A JOURNAL OF THE AMERICAN CHEMICAL SOCIETY

pubs.acs.org/JPCA Article

Identification of Isoprene Oxidation Reaction Products via Anion Photoelectron Spectroscopy

Marissa A. Dobulis, Michael C. Thompson, and Caroline Chick Jarrold*

Cite This: J. Phys. Chem. A 2021, 125, 10089−10102 Read Online

ACCESS | Metrics & More | Article Recommendations | Supporting Information

ABSTRACT: We present a study on the oxidation of isoprene under several different conditions that may model both atmospheric and combustion chemistry. Anions, formed by passing isoprene/oxidant gas mixtures through a pulsed discharge generating a range of species, are separated via mass spectrometry and characterized by anion photoelectron (PE) spectroscopy supported by computations. Specifically, a UV-irradiated isoprene/O_2 mixture, which additionally produces O_3, and an isoprene/O_2/H_2 mixture, which generates $^{\bullet}$OH when passed through the discharge, were sampled. The mass spectra of ions generated under both conditions show the production of intact molecular ions, ion−molecule complexes (e.g., O_2^-, O_4^-, and O_2^-·isoprene), and singly deprotonated species (e.g., deprotonated isoprene, $C_5H_7^-$). In addition, both smaller and oxidized fragments are observed using both gas mixtures, though relative abundances differ. From the UV-irradiated isoprene/O_2 gas mixture, additional intact molecular products of reactions initiated by ozonolysis of isoprene, methylglyoxal, and dimethylglyoxal were observed. Fragmentation and oxidation of isoprene observed in both gas mixtures included species with m/z 39, 53, 67, 69, and 83 that we attribute to a series of alkyl- and alkenoxide-based anions. The coexistence of intact molecules and complexes with fragments and reaction products demonstrates the versatility of this ion source as a simple and efficient anion formation method for studying species that may be relevant in atmospheric and combustion chemistry.

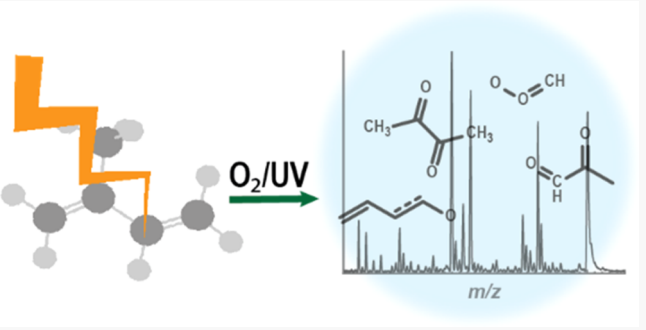

INTRODUCTION

Many species generated via the combustion of hydrocarbons impact both global climate and air quality upon emission into the atmosphere. Biomass emissions are well known to result in the formation of both primary organic aerosols[1,2] and precursors to secondary aerosols.[3] Furthermore, soot and other combustion products have adverse effects on human health.[4,5] However, mechanisms for soot formation are not fully understood, although previous studies have suggested that polycyclic aromatic hydrocarbons (PAHs) are responsible.[6−10] These PAHs are produced by the formation of what is called the "first aromatic ring", which include benzene,[11,12] napthalene,[13,14] and other rings.[15−20] Recently, Johansson et al. suggested a mechanism for the formation of soot from PAHs where small resonance-stabilized radicals produced in combustion can chain-link to irreversibly form large molecular clusters that become soot.[21] This has been predicted to result in the formation of a variety of large ring structures.[22−24] Understanding the electronic structures of small, conjugated radicals and other oxidative products of anthropogenic and biogenic hydrocarbons to aid in kinetic and atmospheric modeling of these processes is therefore important.

The most prevalent nonmethane hydrocarbon in the atmosphere is isoprene.[25] In this report, we present and characterize anions resulting from passing isoprene (2-methyl-1,3-butadiene)/oxidant gas mixtures through a pulsed discharge setup using both mass spectrometry and anion photoelectron (PE) spectroscopy. This study represents an extension of our previous studies on the O_2^-·isoprene and OH^-·isoprene ion−molecule complexes (IMCs).[26,27] What we describe below are ions resulting from fragmentation, some of which undergo further oxidation reactions, rather than simple ion−molecule associations. As described below, two oxidizing gas mixtures were explored for generating product anions.

The prevalence of isoprene in atmospheric chemical processes motivates this current study. The choices of oxidizing gas mixtures, which generate $^{\bullet}$OH and ozone, were also motivated by atmospherically relevant reactions of these radicals with isoprene. $^{\bullet}$OH is the primary tropospheric oxidizer of isoprene,[28,29] and ozone is the second-most prevalent oxidizer of isoprene (although at a much lesser percentage of total isoprene reactions).[28] The reaction of

Received: September 16, 2021
Revised: November 1, 2021
Published: November 10, 2021

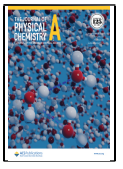

https://doi.org/10.1021/acs.jpca.1c08176
J. Phys. Chem. A 2021, 125, 10089−10102

isoprene with •OH accounts for ∼85% of isoprene's reactive fate and contributes to its average atmospheric lifetime of only 1−2 h.[30] The reactions of isoprene and ozone have been more difficult to fully characterize due to uncertainty in kinetic measurements[31,32] and the relatively low percentage of isoprene + ozone reactions out of all isoprene reactions, but isoprene ozonolysis forms a wide variety of products and is a known ozone loss mechanism in areas of high isoprene concentrations.[33] As such, identifying potential products of these reactions (especially in a high-temperature regime, which could be consistent with the conditions observed in combustion) of both reactions is of significant importance.

Beyond the interest in the oxidation of isoprene via atmospheric chemical processes or in combustion, the speciation of molecular and complex ions generated in electrical discharges is of secondary interest from an experimental standpoint. Electrical discharges are well known to produce a variety of cationic,[34−36] anionic,[37−44] and neutral[45,46] products from simple hydrocarbons or other small molecules as starting materials, resulting in complex mass spectra. Many of these ions and their corresponding reactive neutrals may be present in interstellar medium.[47−49] Consequently, these species of potential astrochemical interest, and the methods by which they are formed, may inform experimental approaches to generating specific conformational isomers, as many interstellar species are otherwise difficult to reproduce in the laboratory setting.

In this study, the anion photoelectron (PE) spectra of m/z 45, 69, 72, 85, and 86 ions formed from UV-irradiated isoprene/O_2 gas mixtures (henceforth referred to as isoprene/O_2/UV) and m/z 53, 67, 69, and 83 generated by isoprene/O_2/H_2 mixtures are reported. Tentative structural assignments are made with supporting density functional theory calculations, giving insights into speciation in the combustion and discharge-induced chemistry of isoprene. We observe hydrogen abstraction and oxygen addition products and describe several potential reaction pathways. We also observe unique products definitively linked to the reaction of ozone with isoprene.

METHODS

Experimental. Anionic species resulting from the oxidation of isoprene under several different conditions were mass-analyzed and spectroscopically probed via anion PE spectroscopy using an anion PE imaging apparatus that has been described previously,[50] and thus only a brief description follows. As noted above, isoprene-based species were generated under several different oxidizing conditions, with ionization achieved by passing the species through a pulsed discharge source described below. As a baseline measurement, a gas mixture of 30% O_2, ∼1% isoprene, and balance Ar (henceforth referred to as isoprene/O_2) was passed through the discharge to determine the prevalence of isoprene fragmentation in the discharge. This method had been used previously to generate the O_2^-·isoprene IMC.[27] Second, the same gas mixture was irradiated with 254 nm light using a mercury lamp (UVP, 90-0012-01) for 10 min prior to expanding the gas through the discharge (i.e., isoprene/O_2/UV). Irradiation of O_2 with UV light generates ozone, which is reactive toward isoprene. Ions generated from expansion of this gas irradiated for different periods of time are included in the Supporting Information. Finally, the isoprene/O_2/H_2 gas mixture was prepared with 27.5% H_2, ∼2% O_2, ∼1% isoprene (Alfa Aesar, 99%), and balance Ar, which generates the oxidizing •OH radical and OH^- ions upon passing through the discharge.[26,51] To reduce the risk of explosion, we systematically added the reagents (isoprene, then O_2, buffer Ar, then H_2, and finally, the remaining Ar) to the electrically grounded tank.

The gas mixtures expanded from a pulsed molecular beam valve (backing pressure 60 psig) and through a needle electrical discharge[52] stabilized by a hot, biased thoriated iridium filament situated ca. 1 cm from the discharge. The expansion was skimmed, and the anions were accelerated to +1 kV and rereferenced to ground[53] before entering a Bakker-style time-of-flight mass spectrometer.[54,55] Anions of a selected m/z were intersected with the second harmonic (532 nm, 2.330 eV) or third harmonic (355 nm, 3.495 eV) of an Nd:YAG laser. The resulting photoelectrons were velocity-mapped onto a two-dimensional microchannel plate detector and phosphor screen,[56,57] and the image was recorded with a CCD camera.[58] Velocity distributions are obtained from the photoelectron images by performing an inverse Abel transformation using the BASEX program,[59] with the image radii to velocity and subsequently electron kinetic energy (e^-KE) calibration performed by measuring the well-known PE spectrum of O_2^-.[60] The e^-KEs are related to the energies of the neutral and anion via

$$e^-KE = h\nu - EA - E_{int}^{neutral} + E_{int}^{anion}$$

where $h\nu$ is the photon energy used to detach the electrons, EA is the adiabatic electron affinity of the neutral, and E_{int}^{anion} and $E_{int}^{neutral}$ are the internal energies (electronic, vibrational, and rotational) of the anion and neutral, respectively. If the anion has low internal energy, the spectrum primarily reflects the neutral energy level spacings. PE spectra are presented in terms of electron binding energy (e^-BE), which is photon energy-independent, and were calibrated by the well-known O_2^- PE spectrum.

Reconstructed images shown in the Supporting Information are performed using the pBASEX program,[61] which do not have centerline artifacts.

Computational. Calculations on a wide range of molecular anions potentially formed under the experimental conditions were performed using the GAUSSIAN 16[62] suite for electron structure calculations to help in species identification. Optimized structures were calculated using the Coulomb-attenuating method-Becke, 3-parameter, Lee, Yang, and Parr (CAM-B3LYP)[63] functional and the aug-cc-pVTZ basis set.[64] Calculated adiabatic detachment energies (ADEs) associated with transitions from global or local minimum energy structures of the various anions to the most similar neutral structures, and which equal the neutral EA when both the anion and neutral are in their ground states, were determined from the difference in the zero-point-corrected total energy of each anion and associated neutral. Vertical detachment energies (VDEs) were determined from the energy difference between the total energy of the initial ion and the associated neutral confined to the structure of the ion. The VDE is the energy of the transition at which the intensity reaches a maximum (highest Franck−Condon overlap). Time-dependent density functional theory (TD-DFT) calculations were also performed at CAM-B3LYP/aug-cc-pVTZ to determine the relative energy of the first excited states of the neutrals. TD-DFT calculations were benchmarked against the well-known term energy (T_0) of the first excited state of the vinoxy radical.[65−67] Both higher-level theory and previous experiments yielded $T_0 \approx 1.00$ (±0.02) eV; TD-CAM-B3LYP/aug-

https://doi.org/10.1021/acs.jpca.1c08176
J. Phys. Chem. A 2021, 125, 10089−10102

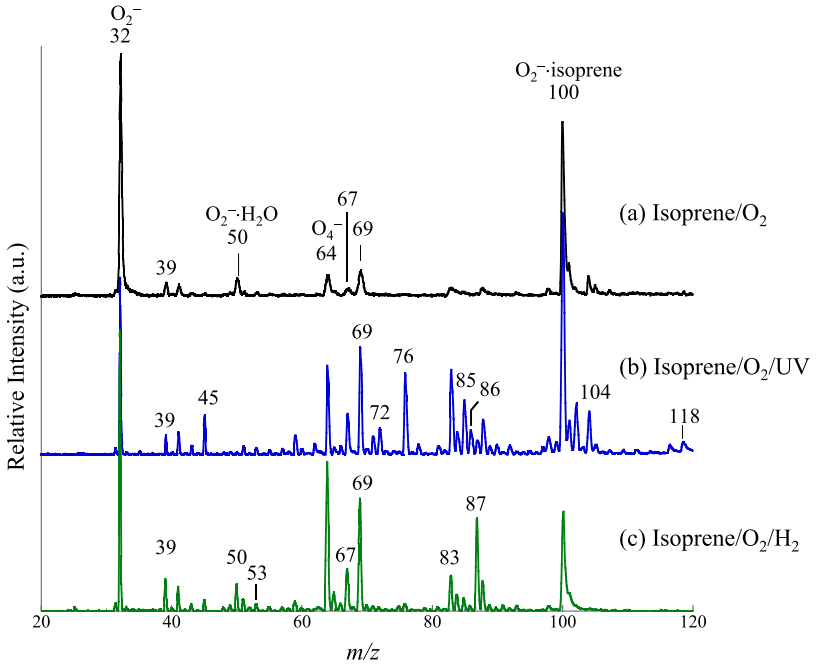

Figure 1. Mass spectra ions generated from discharge through the (a) isoprene/O_2, (b) isoprene/O_2/UV, and (c) isoprene/O_2/H_2 gas mixtures described in the text. Ions are labeled by m/z.

cc-pVTZ calculations yield a first term energy of 1.45 eV, while more expensive equation-of-motion coupled-cluster (EOM-CCSD) previously shown to be effective in treating open-shell species[68] excited-state calculations (using the CAM-B3LYP optimized structure) yields 1.6 eV. Consequently, TD-DFT calculations are used only for *qualitative* assignment of spectra.

To compare experimental and computational results in more detail in the case of the isoprene/O_2/H_2 products, simulations were performed using a home-written Franck−Condon simulation code.[69] Vibrational wave functions were approximated as harmonic oscillator wave functions, and the parallel mode approximation was assumed. However, in the cases of m/z 53 and 67, for which the calculations predict large structural differences between the various isomers of the anion and their associated neutrals, along with floppy and therefore anharmonic neutrals, we instead approximated the transition as a Gaussian distribution that is consistent with the calculated ADE and VDE.

RESULTS

Figure 1a shows the characteristic mass spectrum of ions resulting from the control isoprene/O_2 gas mixture, Figure 1b shows the characteristic snapshot of the mass spectrum anions from the isoprene/O_2 mixture irradiated by a UV lamp variation (isoprene/O_2/UV), and Figure 1c shows the mass spectrum for the isoprene/O_2/H_2 gas mixture. In all three cases, O_2^- and O_2^-·isoprene, appearing at m/z 32 and 100, respectively, are predominant, and O_4^- (m/z 64) is present. O_2^-·H_2O (m/z 50) is also observed in all three mass spectra, though the abundance is very small from the isoprene/O_2/UV variant. The distributions of ions generated with the non-irradiated isoprene/O_2 gas mixture are the simplest; the addition of UV light or H_2 results in a more diverse distribution of species, several of which are common between all three but with different relative abundances. The isoprene/O_2/H_2 gas mixture required higher discharge voltages (ca. 1.8 kV) to produce ions than the isoprene/O_2 mixes (ca. 1.4 kV), which is expected to result in more molecular fragmentation.

Species other than O_2^-, O_4^-, and O_2^-·H_2O and appearing with m/z below 68 are necessarily anions of isoprene fragments, some of which have apparently undergone oxidation (*vide infra*). As examples, the presence of m/z 39 ($C_3H_3^-$), 41($C_3H_5^-$), and 67 ($C_5H_7^-$) in all three panels shows that the discharge source does fragment isoprene while operating at both discharge voltages. Nonetheless, the most abundant species are intact precursor O_2^- or the O_2^-·isoprene IMC.

Isoprene/O_2/UV Products. The mass spectrum of species formed by passing the isoprene/O_2/UV gas mixture through a pulsed discharge shown in Figure 1b is a snapshot of the isoprene + O_3 + O_2 reaction mixture as it evolves in a stagnating gas cell. As the amount of time isoprene/O_2 is held under UV irradiation increases, the relative intensities of ions with m/z 81−93 increase and the ion signal with m/z 76 becomes more prominent, as shown in the Supporting Information (Figure S1). The relative intensity in the ions with m/z 39 and 45 (which are attributed to $C_3H_3^-$ for m/z 39 and potentially $HCOO^-$ for m/z 45, as described below) changes subtly: with increasing UV exposure time, m/z 45 increases in intensity relative to m/z 39. Low-intensity species with odd m/z between 51 and 59 increase marginally as the exposure time increases as well.

Again, there are numerous species that appear in the mass spectra obtained under conditions (b) and (c), e.g., m/z 39, 69, and 83. However, several species that are more pronounced in the isoprene/O_2/UV mass distribution appear at m/z 45, 72, 76, 85, and 86.

As a first step in identifying these species, we consider the anion PE spectra of species with m/z 72 and 86, as these m/z values coincide with methylglyoxal and dimethylglyoxal (biacetyl), saturated species that are known to bind an electron, forming radical anions.[70,71] The spectra obtained using 3.495 eV photon energy are shown in Figure 2a,b. Raw and reconstructed images are included in the Supporting

https://doi.org/10.1021/acs.jpca.1c08176
J. Phys. Chem. A 2021, 125, 10089−10102

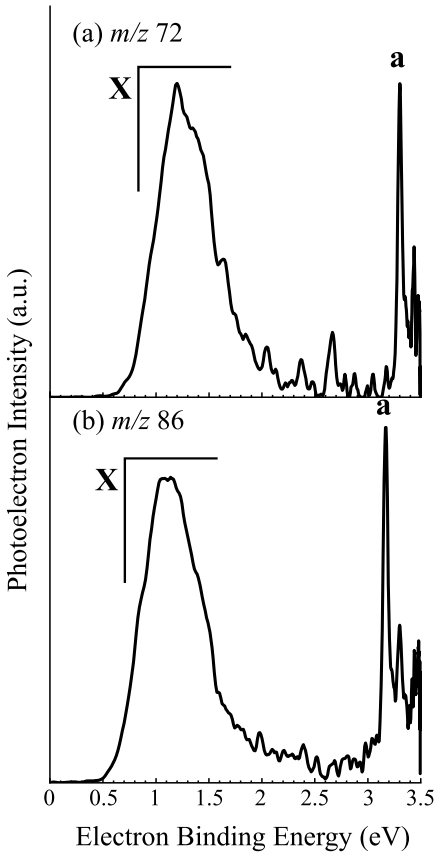

Figure 2. 3.495 eV PE spectra of the ions with (a) m/z 72 and (b) m/z 86 generated from discharge through the isoprene/O_2/UV gas mixture.

Information. Both spectra are similar, showing broad transitions lying between approximately 0.7 and 2 eV (band **X**), with narrower features (band **a**) lying above e$^-$BE values of 3 eV. Transition energies are summarized in Table 1. These spectra are identical to that of the methylglyoxal and dimethylglyoxal spectra measured previously by Sanov and co-workers.[70,71] Bands **X** and **a** correspond to the $X\ ^1A' \leftarrow X\ ^2A''$ and $a\ ^3A'' \leftarrow X\ ^2A''$ transitions in methylglyoxal and the $X\ ^1A_g \leftarrow X^2A_u$ and $a\ ^3A_u \leftarrow X^2A_u$ in dimethylglyoxal. We further confirmed the latter by measuring the spectrum of the anion generated by expanding dimethylglyoxal seeded in O_2 and Ar; this spectrum is shown superimposed on the isoprene/O_2/UV-generated m/z 86 spectrum in the Supporting Information.

Methylglyoxal is an oxidative product of isoprene in the ozonolysis of methyl vinyl ketone or the reaction of hydroxyl radical with methacrolein and methyl vinyl ketone.[32] The appearance of methylglyoxal further suggests that isoprene becomes increasingly oxidized by this gas mixture in our discharge ion source. We note that the ion with m/z 58, which could correspond to the glyoxal anion (the smallest of this dicarbonyl family and a distant oxidative product of isoprene),[32] is not observed in large quantities in the mass spectrum. The appearance of dimethylglyoxal is of interest, as dimethylglyoxal has been observed in the reactions of methyl vinyl ketone and methacrolein, two immediate products in the ozonolysis of isoprene, with the hydroxyl radical through an unknown mechanism.[72] We note that the methacrolein oxide and methyl vinyl ketone oxide Criegee intermediates, which are produced in the ozonolysis of isoprene and would have the same m/z as dimethylglyoxal, do not appear to contribute to the PE spectrum.

Table 1. Summary of Experimental Results Observed in the PE Spectra of m/z 45, 69, 72, 85, and 86 from the Isoprene/O_2/UV Reactions and m/z 53, 67, 69, and 83 from the Isoprene/O_2/H_2 Radical Reactions

		isoprene/O_2/UV		
m/z	band	ADE (eV)	VDE (eV)	assignment
45	X	2.42 ± 0.05	2.98 ± 0.05	$HCOO^-$
69	X	1.88 ± 0.05	2.00 ± 0.05	$C_4H_5O^-$
	X′	0.8 ± 0.1	1.14 ± 0.05	unknown
72	X	0.9 ± 0.1	1.20 ± 0.05	methylglyoxal$^-$ $X\ ^1A' \leftarrow X\ ^2A''$
	a	3.28 ± 0.02		methylglyoxal$^-$ $a\ ^3A'' \leftarrow X\ ^2A''$
85	X	2.70 ± 0.05	3.02 ± 0.05	*tent.* $C_4H_5O_2^-$
86	X		1.18 ± 0.05	dimethylglyoxal$^-$ $X\ ^1A_g \leftarrow X\ ^2A_u$
	a		3.18 ± 0.05	dimethylglyoxal$^-$ $a\ ^3A_u \leftarrow X\ ^2A_u$
		isoprene/O_2/H_2		
39	X	1.02 ± 0.05	1.33 ± 0.05	$C_3H_3^-$
53	X	0.78 ± 0.10	1.23 ± 0.05	$C_4H_5^-$
67	X	0.63 ± 0.05	0.77 ± 0.05	$C_5H_7^-$
	X′		1.94 ± 0.05	$C_4H_3O^-$ (furanide)
69	X	1.92 ± 0.05	2.00 ± 0.05	$C_4H_5O^-$
83	X	1.77 ± 0.05	1.87 ± 0.05	$C_5H_7O^-$

The m/z 76 anion did not detach using 3.495 eV, suggesting a highly oxidized species. Constraining assignment of this ion to a $C_xH_yO_z^-$ stoichiometry, $C_6H_4^-$, C_5O^-, $C_3H_8O_2^-$, $C_2H_2O_3^-$, or CO_4^- are all possibilities. $C_6H_4^-$ seems less likely because it would require association between two fragments of isoprene, C_5O^- is unlikely because no other singly oxidized carbon clusters are observed, and $C_3H_8O_2^-$ is hyper-reduced compared to, for example, methylglyoxal or dimethylglyoxal. $C_2H_2O_3^-$ may be assigned to 1,2,3-trioxolane or 1,2,4-trioxolane, stable species formed in reactions with ozone, and CO_4^- would be a strongly bound $[O_2\text{-}CO_2]^-$ complex, which has a VDE of 4.56 eV, above the photon energy used in this experiment.[73] Support for assigning m/z 76 to $[O_2\text{-}CO_2]^-$ is in the appearance of ions at m/z values corresponding to $[O_2\text{-methylglyoxal}]^-$ (m/z 104) and $[O_2\text{-dimethylglyoxal}]^-$ (m/z 118) in Figure 1b. These anionic complexes are more strongly bound than simple IMCs because of charge transfer between the O_2^- and the C-centers of the partner molecule.[74]

We will now consider the PE spectra of the other species that are generated under the same source conditions as the methylglyoxal and dimethylglyoxal anions. The PE spectra of species with m/z 45, m/z 69, and m/z 85 are shown in Figure 3a–c, respectively. All spectra were collected using 3.495 eV photon energy.

Both $C_2H_5O^-$ and CHO_2^- have m/z 45. However, based on the appearance of the PE spectrum in Figure 3a, we can eliminate the possibility that it is the ethoxide anion. Ellison and co-workers,[75] and Continetti and co-workers,[76] determined the EA of the ethoxy radical to be 1.726 eV, whereas the EA of the m/z 45 ion produced here is 2.50 ± 0.01 eV (transition energies summarized in Table 1). This EA is significantly lower than that of formoxyl radical, 3.498 ± 0.015 eV,[77] and greater than that of *cis*-or *trans*-HOCO, 1.51 and 1.37 ± 0.01 eV, respectively.[78]

https://doi.org/10.1021/acs.jpca.1c08176
J. Phys. Chem. A 2021, 125, 10089−10102

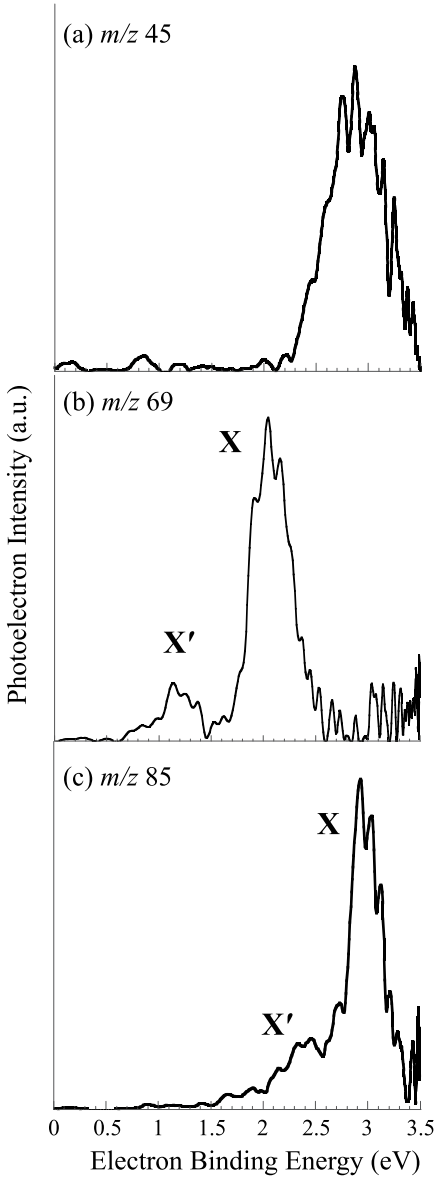

Figure 3. 3.495 eV PE spectra of the ions with (a) m/z 45, (b) m/z 69, and (c) m/z 85 generated from discharge through the isoprene/O_2/UV gas mixture.

Results of calculations on the neutral radicals HCOO, COOH, $HOCH_2CH_2$, and $HOCHCH_3$ and their associated anions are summarized in the Supporting Information. The ethanol radicals are predicted to be either negative or very low EAs. The *cis*-$COOH^{(-)}$ conformer rearranged to form $HOCO^{(-)}$ in all optimizations and were calculated to have similar EAs determined previously by Johnson et al.[78] The *trans*-COOH was calculated to have an EA of 0.18 eV, well below the experimental value. However, the lowest overall energy conformer, $HCOO^-$, was calculated to have an EA of 2.68 and 2.60 eV for cis- and trans- conformers, respectively, in good agreement with the m/z 45 spectrum. The HCOO anion structures are shown in Figure 4a, and their relative energies are included in Table 2. This ion is similar to formaldehyde oxide (CH_2OO), which is a primary reaction product in the ozonolysis of isoprene (or any partially or fully unsubstituted alkene). The relatively high abundance of this species in Figure 1b, when compared to the intensity of m/z 45 generated under the other ion source conditions, therefore suggests ozonolysis of isoprene. Loss of a proton, or loss of H-atom with subsequent electron attachment, is suggested from the appearance of m/z 67 in the mass spectrum of anions generated from the control isoprene/O_2 gas mixture (Figure 1a); a similar process may lead to the formation of $CHOO^-$ from CH_2O_2.

Isoprene ozonolysis resulting in species with a single carbon atom, like those that could account for m/z 45, would also result in species with four carbon atoms. The ion observed with m/z = 69, which is present in the mass spectra shown in Figure 1a−c, is consistent with $C_4H_5O^-$. It is one mass unit lighter than methyl vinyl ketone or methacrolein, both of which are primary products in the tropospheric reaction of isoprene with ozone. The spectrum shown in Figure 3b exhibits two distinct transitions. The lower-energy, lower-intensity transition labeled **X′** has an origin of 0.8 ± 0.1 eV and a VDE of 1.14 ± 0.05 eV, and the intense transition, **X**, has an origin of 1.88 ± 0.05 eV and a VDE of 2.00 ± 0.05 eV. The energy and spectral profile of band **X** are consistent with the PE spectrum of an alkenoxide,[79−82] whereas band **X′** requires further explanation.

$C_5H_9^-$ would also appear at m/z 69, though calculations (Supporting Information) predict the EA of the various structural isomers to be approximately 0.4 eV, below the observed signal. Moreover, given the abundance of oxidizing agents in the gas mix, a species that is incrementally more reduced than isoprene seems unlikely. A summary of other calculated $C_4H_5O^-$ structures and energies is included in the Supporting Information, and the two lowest-energy structures of the anion are shown in Figure 4b. Oxygen addition to the C_4H_5 radical at C1 [buta-1,3-dien-1-oxide (**I**)] is lower in energy than the C2 analogue [buta-1,3-dien-2-oxide (**II**)] by 0.39 eV, though the formation of **I** requires additional rearrangement relative to ozonolysis of the C1−C2 bond with methyl group deprotonation suggested by structure **II**. The calculated ADEs for **I** and **II** are 1.88 and 1.90 eV, respectively, both in relatively good agreement with band **X**. Assignment of band **X′** remains uncertain. We cannot exclude the possibility that long-lived electronically excited states of any possible species with m/z 69 may be populating ion beam and contributing to this lower e^-BE band.

Figure 3c shows the PE spectrum of an anion with m/z 85, which is mass-coincident with the OH^-·isoprene IMC produced using the isoprene/O_2/H_2 gas mix, studied previously.[26] The spectrum shown here is additional evidence of disparate speciation between the different ion source conditions and reactants used in this study, as it is different from the spectrum assigned to the IMC (the two distinct spectra are shown superimposed in the Supporting Information). The lower-intensity band **X′** is situated over an e^-BE range consistent with an ensemble of different alkenoxides populating the beam. However, the dominant feature band **X** in the spectrum is observed at a VDE of 3.02 eV, significantly higher than the 2.45 eV VDE observed in the PE spectrum of the mass-coincident IMC. Again, considering that the isoprene/O_2/UV conditions have much higher concentrations of O_2 and O_3 relative to the isoprene/O_2/H_2 gas mixture, and given the typical alkenoxy radical EA of *ca.* 1.9 eV,[75,76,79−82] we suggest that this species has a more oxidized composition, such as $C_4H_5O_2^-$, particularly as m/z 85 is 16 units heavier than the abundant m/z 69 anion. For comparison, the EA of acetyloxyl radical is 3.250 ± 0.010 eV.[83]

https://doi.org/10.1021/acs.jpca.1c08176
J. Phys. Chem. A 2021, 125, 10089−10102

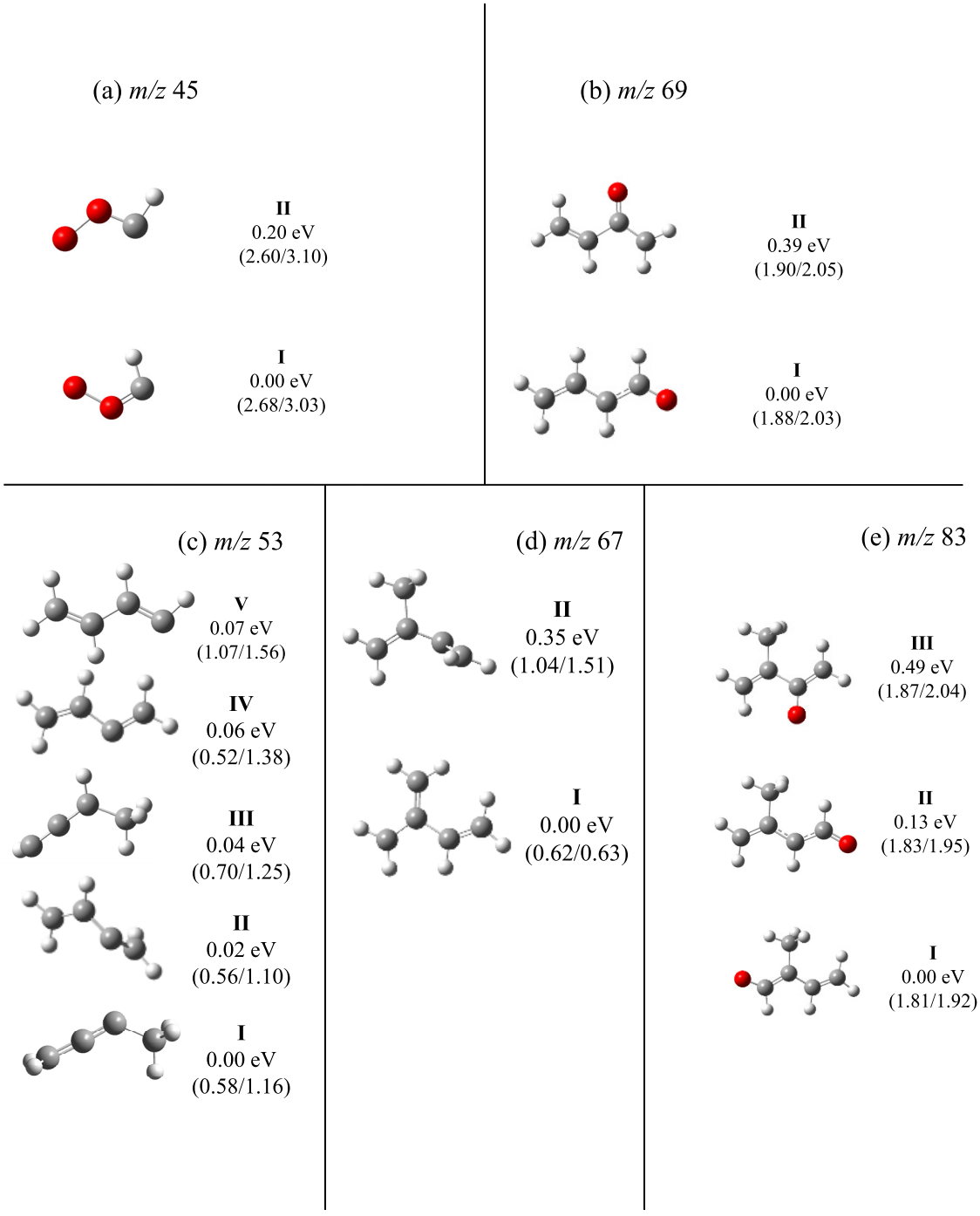

Figure 4. Lowest-energy structures calculated to be most consistent with the observed PE spectra of anions with (a) 45, (b) 69, (c) 53, (d) 67, and (e) 83. Calculations were performed at the CAM-B3LYP/aug-cc-pVTZ level of theory.

Isoprene/O_2/H_2 Products. The PE spectra of anions generated using the isoprene/O_2/H_2 gas mixture are broken into two groups based on the differences in EA of the resulting neutrals, as described in more detail below. The spectra of ions appearing at m/z 39, m/z 53, and m/z 67 are shown in Figure 5a–c, respectively. In addition to the PE spectrum of m/z 67 obtained using 3.495 eV photon energy (Figure 5c), the spectrum obtained using 2.330 eV, along with several spectral simulations (*vide infra*), is shown in Figure 5d.

Figure 6a shows the PE spectrum obtained for m/z 69 (black trace) and Figure 6b shows the PE spectrum obtained for m/z 83 (black trace), both using 2.330 eV photon energy. Red and blue traces are simulations described below. The spectra obtained using 3.495 eV photon energy do not exhibit any additional features at higher e^-BEs and are therefore included in the Supporting Information.

Note that there is a difference between the spectrum of m/z 69 shown in Figure 6a and of that described in the previous section and shown in Figure 3b. Raw and reconstructed images are included in the Supporting Information. ADE and VDE values for transitions observed in the spectra are summarized in Table 1.

Alkyl radical species typically have modest EAs below 1 eV,[84−87] while alkoxy and alkenoxy radicals have EAs in the

https://doi.org/10.1021/acs.jpca.1c08176
J. Phys. Chem. A 2021, 125, 10089−10102

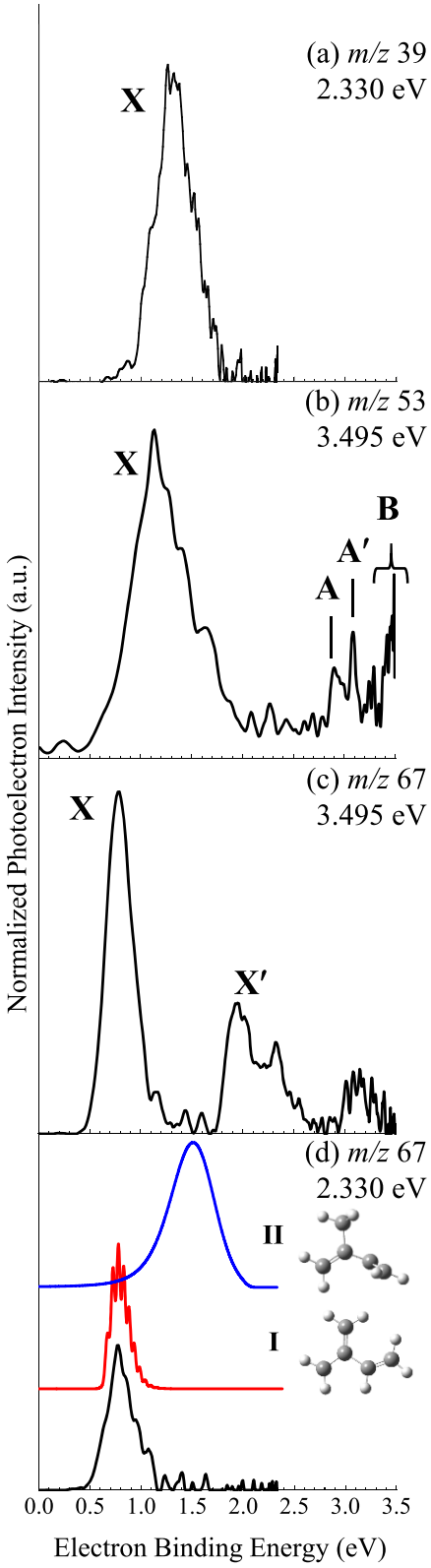

Figure 5. PE spectra of the ions with (a) m/z 39 ($h\nu$ = 2.330 eV), (b) m/z 53 ($h\nu$ = 3.495 eV), and m/z 67 obtained with both (c) $h\nu$ = 3.495 eV and (d) $h\nu$ = 2.330 eV (black traces) generated from discharge through the isoprene/O_2/H_2 gas mixture. Panel (d) includes simulations based on computed structures of $C_5H_7^-$ **I** (red trace) and **II** (blue trace) shown in Figure 4d. Simulation parameters are given in the Supporting Information.

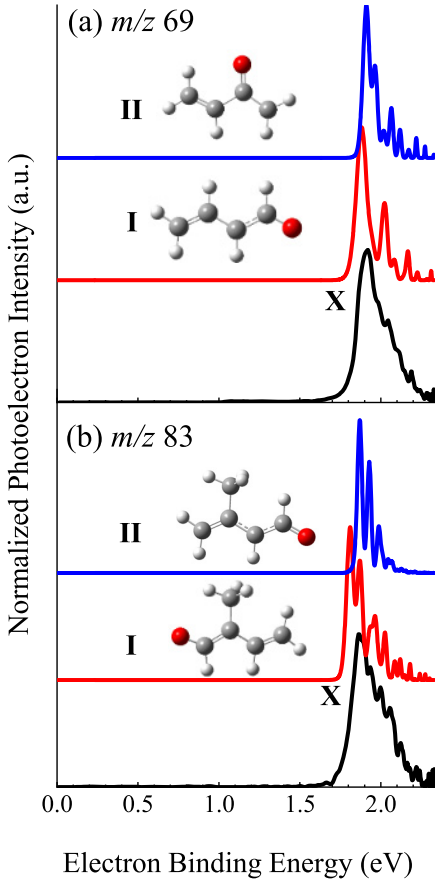

Figure 6. PE spectra of the ions with (a) m/z 69 and (b) m/z 83 measured with $h\nu$ = 2.330 eV (black traces) generated from discharge through the isoprene/O_2/H_2 gas mixture. Simulations based on the two lowest-energy isomers calculated for the anions are shown above each experimental spectrum. In panel (a), the simulated spectra correspond to structures **I** (red trace) and **II** (blue trace) in Figure 4b. In panel (b), the simulated spectra are based on structures **I** (red trace) and **II** (blue trace) in Figure 4e. Simulation parameters and spectra obtained using $h\nu$ = 3.495 eV photon energy are included in the Supporting Information.

1.8−2 eV range.[79−82] Given the H_2-rich composition of the gas mixture, the lower O_2 concentration relative to the isoprene/O_2/UV ion source conditions, along with the known typical alkyl and alkoxy radical EAs, we suggest that the m/z 39, m/z 53, and m/z 67 ions, the spectra of which are shown in Figure 5a−c respectively, correspond to (a) $C_3H_3^-$, (b) $C_4H_5^-$, and (c) $C_5H_7^-$, and the m/z 69 and m/z 83 ions, the PE spectra of which are shown in Figure 6a,b, respectively, are $C_4H_5O^-$ and $C_5H_7O^-$. The PE spectra of both $C_4H_5^-$ and $C_5H_7^-$ exhibit features at higher e$^-$BE values, which will be addressed below.

Alkyl Radicals. The presence of $C_5H_7^-$ (m/z 67) is evocative of H abstraction from isoprene by $^\bullet$OH generated in the discharge followed by electron attachment, while $C_4H_5^-$ (m/z 53) is evocative of methyl loss from isoprene followed by electron attachment. However, the presence of $C_3H_3^-$ suggests that other indirect pathways of ion formation are occurring; the spectrum of $C_3H_3^-$ is very similar in profile to that of the allenyl anion ($H_2C{=}C{=}C{-}H^-$) reported by Ellison and co-workers[87] and Lineberger and co-workers.[88] The neutral EA was reported to be 0.918 eV, and the VDE was 1.3 eV. Its formation from isoprene fragmentation would minimally

https://doi.org/10.1021/acs.jpca.1c08176
J. Phys. Chem. A 2021, 125, 10089−10102

Table 2. Summary of Computational Results of the Neutral/Anion Pairs of Interest Calculated at CAM-B3LYP/aug-cc-pVTZ. Isoprene/O_2/UV and isoprene/O_2/H_2 contributing species are divided by the double line

isomer		species	energy relative to lowest-energy anion (eV)	EA (eV)	VDE (eV)
C_4H_5O	neutral	buta-1,3-dien-2-oxy (**II**)	2.30	1.90	2.05
		buta-1,3-dien-1-oxy (**I**)	1.88	1.88	2.03
	anion	buta-1,3-dien-2-oxide (**II**)	0.39		
		buta-1,3-dien-1-oxide (**I**)	0.00		
HCOO	neutral	*trans*-HCOO (**II**)	2.80	2.60	3.10
		cis-HCOO (**I**)	2.68	2.68	3.03
	anion	*trans*-$HCOO^-$ (**II**)	0.20		
		cis-$HCOO^-$ (**I**)	0.00		
C_4H_5	neutral	*t,t*-1,3-butadien-1-yl (**V**)	1.14	1.07	1.56
		but-1-yn-3-yl (**III**)	0.74	0.70	1.25
		but-2-yn-1-yl (**I**)	0.58	0.58	1.16
		1,2-butadien-4-yl (**II**/**IV**)	0.58	0.56/0.52	1.10/1.38
	anion	*t,t*-1,3-butadien-1-ide (**V**)	0.07		
		1,2-butadien-4-ide (**IV**)	0.06		
		but-1-yn-3-ylide (**III**)	0.04		
		1,3-butadien-2-ide (**II**)	0.02		
		but-2-yn-1-ylide (**I**)	0.00		
C_5H_7	neutral	2-methyl-1,3-butadien-3-yl (**II**)	1.41	1.04	1.51
		2-methylene-1,3-butadienyl (**I**)	0.62	0.62	0.63
	anion	2-methyl-1,3-butadien-3-ide (**II**)	0.35		
		2-methylene-1,3-butadienide (**I**)	0.00		
C_5H_7O	neutral	1,4-butadien-2-methyloxy (**IV**)	3.49	1.90	2.06
		3-methyl-1,3-butadien-2-oxy (**III**)	2.36	1.87	2.04
		3-methyl-1,3-butadien-1-oxy(**II**)	1.96	1.83	1.95
		2-methyl-1,3-butadien-1-oxy (**I**)	1.81	1.81	1.92
	anion	1,4-butadien-2-methyloxide (**IV**)	1.59		
		3-methyl-1,3-butadien-2-oxide (**III**)	0.49		
		3-methyl-1,3-butadien-1-oxide (**II**)	0.13		
		2-methyl-1,3-butadien-1-oxide (**I**)	0.00		

require two steps (e.g., C2−C3 bond fission with H_2 loss from the methyl group).

We therefore consider the PE spectra in more detail, along with the computational results, to determine whether the molecular structures of the $C_5H_7^-$ and $C_4H_5^-$ anions are formed directly from −H or $-CH_3$ loss, respectively, from isoprene, or if the structures are formed by a more complex process.

The PE spectrum of m/z 53 (Figure 5b) exhibits a broad electronic transition (**X**) with an EA of 0.78 ± 0.10 eV and a VDE of 1.23 ± 0.05 eV. The spectrum shows additional lower-intensity transitions centered at 2.80 ± 0.05 and 3.04 ± 0.05 eV, labeled **A** and **A′**, respectively, and a signal near threshold labeled **B**. The spectrum obtained using 2.330 eV photon energy is shown on an expanded scale in the Supporting Information, along with low-energy structures determined computationally for the anion and associated neutrals accessible via one-electron detachment of the anions.

Several energetically competitive structures calculated for $C_4H_5^-$ are shown in Figure 4c. Simulations based on these structures are vibrationally broadened and unresolved, are very similar in appearance, and are therefore placed in the Supporting Information. Five low-energy structural isomers of the anion were found to lie within a 0.07 eV energy window; it is therefore not possible to assert which is the true lowest-energy isomer based on the calculations.

By a small margin, the lowest-energy anion is calculated to be an alkyne structure [but-2-yn-1-ylide (**I**) anion]. The 1,3-butadien-2-ide (**II**) structure is predicted to be 0.02 eV higher in energy, with the but-1-yn-3-ylide (**III**) and two more butadiene-based structures [1,2-butadien-4-ide (**IV**) and *t,t*-1,3-butadien-1-ide (**V**)] several hundredths of an eV higher. Anion structures **I** and **III** both have a terminal methyl group. The associated radical neutral structure for anion **I** converged to be linear along the C1−C2−C3 bond, as shown in the Supporting Information, with a computed EA of 0.58 eV, 0.2 eV below the observed spectral origin. Neutral structure **III** optimized with an EA of 0.70 eV. Neutral TD-DFT calculations were performed on both **I** and **III** confined to the structures of their associated anions, and the lowest-lying excited states were predicted to be at e^-BE values (term energy plus EA) 3.32 and 3.50 eV for isomers **I** and **III**, respectively, which are above the e^-BEs of features **A** or **A′**. Relative energies, ADEs, and VDEs are summarized in Figure 4c and Table 2.

Structures **II** and **IV** of $C_4H_5^-$ are nonplanar and planar conformers, respectively, of a structure formed by simple methyl group elimination from isoprene. Structure **IV** is calculated to be 0.04 eV higher in energy than **II**, and the barrier for interconversion from **II** to **IV** is calculated to be 0.09 eV (transition-state structure shown in the Supporting Information), which is below the internal energy of this polyatomic at 300 K. The nonplanar structure **II** is similar to the nonplanar intermediate previously predicted in the transition from 1,3-butadien-2-yl to 1,2-butadien-4-yl.[89,90] The neutral radicals associated with **II** and **IV** converged to a common 1,2-butadien-4-yl structure, in agreement with previous reports.[89] Our optimizations of the previously

https://doi.org/10.1021/acs.jpca.1c08176
J. Phys. Chem. A 2021, 125, 10089−10102

reported trans neutral geometry, which were calculated by Parker and Cooksy at QCISD and UHF levels of theory,[89] converged to the transition state using the CAM-B3LYP level of theory. Calculated relative energies, ADEs, and VDEs of these radical neutrals and closed-shell anions are summarized in Table 2. TD-DFT calculations on the neutral confined to the geometry of the anion for the 1,2-butadien-4-ide **II** and **IV** predicted the lowest-lying excited states to lie at e$^-$BE values of 3.12 and 2.30 eV, respectively, with the former in good agreement with the position of **A** and **A′** in the 3.495 eV spectrum. However, band **B** remains unassigned.

Finally, anion structure **V** could form from methyl loss from isoprene followed by hydrogen transfer from C1 to C2; it is also planar. However, the EA of the associated neutral radical is calculated to lie 0.3 eV above the observed transition. Structure **V** is the only species that can be eliminated with certainty. Structure **II** formed by simple methyl loss from isoprene has excited-state energies that are consistent with the higher-lying transitions observed in the experimental spectrum. However, the EAs and VDEs calculated for structures **I** through **IV** are all in reasonable agreement with band **X** in the PE spectrum.

Calculations on C_3HO^-, which is mass-coincident with $C_4H_5^-$, predicted much higher electron binding energies. Four structures of C_3HO^- with relative energies are included in the Supporting Information. The lowest-energy anion ($CCCHO^-$) has a neutral EA of 3.99 eV, above the photon energy used in this study. The other anion structures were predicted to be 0.48−1.99 eV higher in energy, with neutral EAs that are inconsistent with the spectrum. As they are much higher in energy, these structures would not likely be abundant in the ion beam.

The PE spectrum of the ion tentatively attributed to $C_5H_7^-$ (m/z 67) shown in Figure 5c exhibits a narrower and lower e$^-$BE transition (**X**) than that of $C_4H_5^-$, with an ADE of 0.60 ± 0.07 eV and a VDE of 0.77 ± 0.05 eV. A partially resolved shoulder progression with a 725 cm^{-1} spacing is observed on the higher e$^-$BE portion of band **X** in the spectrum collected using 2.330 eV photon energy, shown in Figure 5d. A lower-intensity band (**X′**) is observed with VDE = 1.95 ± 0.05 eV in the 3.495 eV spectrum. Band **X′** is consistent with the previously reported spectrum of the m/z coincident furanide ($C_4H_3O^-$) ion.[91,92] Furanide signal was more prevalent using lower discharge voltages (1.5 kV) though it was never completely eliminated by increasing the voltage. The low-intensity signal near 3.1 eV is background noise that could not be completely subtracted. It is not symmetric around the image center and can therefore be eliminated as a true signal.

Calculations were done on structures formed by isoprene undergoing hydrogen abstraction from C1, C3, C4, or the methyl group. The two lowest-energy isomers found computationally are shown in Figure 4d. Hydrogen abstraction at the methyl group to form 2-methylene-1,3-butadiene (**I**) yields the lowest relative energy anion (and this C−H bond is the weakest in the molecule), followed by hydrogen abstraction at C_3, forming structure **II** predicted to be 0.35 eV higher in energy. Relative energies are summarized in Table 2. Structures and relative energies of structures formed by C1 and C4 −H abstraction are included in the Supporting Information. The C1, C4, and methyl hydrogen abstraction products have nearly fairly planar backbones present in *trans*-isoprene, while the C3 product is more similar to the *gauche*-isoprene transition state (C1−C2−C3−C4 dihedral angle of ∼80°).[89] The C1 and C4 abstraction anions are calculated to be 0.5−0.7 eV higher in energy than structure **I**.

Neutral structure **I** is planar along the carbon backbone, while the anion is slightly nonplanar, which is consistent with a nearly vertical transition, as reflected in the VDE calculated to be very close to the ADE. In contrast, neutral structure **II** is planar along the butadiene backbone, while anion **II** is nonplanar. The large structural change predicted in the detachment transition results in a substantial energy difference between ADE and VDE values (i.e., a broad Franck−Condon profile), as summarized in Table 2. This is further illustrated by Figure 5d, which shows the PE spectrum of the ion with m/z 67 obtained with 2.330 eV photon energy (black trace) along with the simulations based on structures **I** (red trace) and **II** (blue trace). Simulation parameters are given in the Supporting Information. The vibrationally broadened transition associated with structure **II** allows elimination of structure **II** in assigning the spectrum.

Alkenoxy Radicals. The 2.330 eV PE spectra of the m/z 69 and 83 anions, shown in Figure 6a,b, respectively, exhibit a single and similarly narrow transition (**X**) at approximately 2 eV, which is typical for alkoxide and alkenoxide PE spectra.[75,76,79−82] These ions correspond to $C_4H_5O^-$ and $C_5H_7O^-$ for m/z 69 and 83, respectively.

Band **X** in the m/z 69 PE spectrum (Figure 6a) has an origin of 1.92 ± 0.05 eV, which is the electron affinity of the radical neutral. A short 500 cm^{-1} progression is partially resolved. Again, the spectrum is similar to other alkoxide and alkenoxide spectra but is not identical to that of the m/z 69 spectrum observed in the isoprene/O_2/UV reaction. Band **X** in Figure 6a can be superimposed onto band **X** in the spectrum shown in Figure 3b (the only distinction is the minor difference in signal to noise). However, the absence of band **X′** in Figure 6a supports the earlier suggestion that band **X′** in the spectrum of m/z 69 generated with isoprene/O2/UV gas mixture is due to a different molecular anion. The two spectra obtained using 3.495 eV are shown superimposed in the Supporting Information.

The increased S/N achieved in the spectrum of $C_4H_5O^-$ using the isoprene/O_2/H_2 gas mixture provides a better point of comparison with simulations generated from the calculated structures (Figure 4a) presented in the previous section. Simulations based on structures **I** (red) and **II** (blue) are shown above the experimental spectrum (black) in Figure 6a and are both in good agreement with the experimental spectrum, though the calculated relative energies would support structure **I**.

The PE spectrum of $C_5H_7O^-$ shown in Figure 6b is similar to the $C_4H_5O^-$ spectrum: it is dominated by one narrow transition (**X**) with an origin of 1.86 ± 0.05 eV. The partially resolved vibrational profile appears to have contributions from two modes.

Oxygen addition to isoprene-based radicals can occur at C1, C2, C3, or C4, or, upon loss of H and subsequent O addition, to the methyl group. Of these, the lowest-energy anion was found to be addition to C1, forming the corresponding anion of an alkoxy radical, 2-methyl-1,3-buta-dien-1-oxide (**I**) shown in Figure 4e, with a calculated ADE of 1.81 eV and a VDE of 1.94 eV. The next lowest-energy anion, C4 addition (3-methyl-1,3-butadien-1-oxide, **II**), lies 0.13 eV higher in energy and has a calculated ADE of 1.83 eV with a VDE of 1.95 eV. C3 addition (3-methyl-1,3-butadien-2-oxide, **III**) anion was 0.49 eV higher in energy than C1. The anion corresponding to

https://doi.org/10.1021/acs.jpca.1c08176
J. Phys. Chem. A 2021, 125, 10089−10102

Scheme 1. Potential Formation of *m/z* 69 via the Reaction between Singlet Oxygen ($^1\Delta_g$) and Isoprene Resulting in C=C Bond Cleavage and Carbonyl Fragments[a]

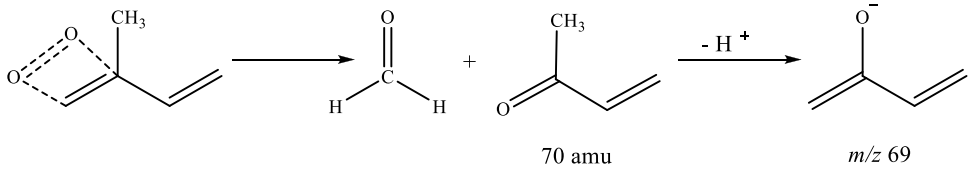

[a]With thermalized electrons present in the ion source, the fragment can undergo dissociative attachment resulting in the net loss of a proton from the methyl group, forming structure **II** (Figure 4b).

oxygen addition to the methyl group (**IV**) is substantially higher in energy, at 1.59 eV higher in energy than the C1 anion, and likely does not contribute to the spectrum. Energies of anion and neutral structures **I**, **II**, **III**, and **IV** are summarized in Table 2. Simulations of a spectrum based on **I** (red trace) and **II** (blue trace) are shown above the experimental spectrum (black trace) in Figure 6b. The simulation based on **III** is compared to that of **I** and **II** in the Supporting Information, though **III** (and **IV**) anions are substantially higher in energy.

While structures **I**, **II**, **III**, and **IV** all have ADEs and VDEs in reasonable agreement with the experimental spectrum, the simulation based on **I** captures the combination bands suggested by the partially resolved profile in the experimental spectrum. As **I** is predicted to be more stable than the other structures, we tentatively assign the spectrum to structure **I**.

The lowest-energy neutral excited state is calculated to be 3.9 eV above the lowest-energy anion, which would not be accessed via detachment with 3.495 eV photon energy.

We also considered the possibility of $C_4H_3O_2^-$, which is *m/z* coincident with $C_5H_7O^-$. Numerous structures for $C_4H_3O_2^-$ were calculated (summarized in the Supporting Information) but all species have computed EAs and VDEs that do not reconcile with the experimental spectrum. We note that the lowest-energy anion of these species has an ADE of 1.98 eV and a VDE of 2.19 eV. While the EA is marginally higher than what is observed experimentally, the ADE−VDE interval is consistent with a broader spectrum. Other $C_4H_3O_2$ structures were calculated to have significantly higher EAs.

DISCUSSION

Pulsed discharge in combination with pulsed molecular beam valves are useful tools in the study of anions, cations, and unstable radical species, though species formed in discharge sources can be surprising in terms of connecting the structures produced by the precursor molecules.[93−95] The results presented above show that the source used in this study produces a combination of fragments, oxidized fragments, and unfragmented species such as the O_2^-·isoprene IMC, methylglyoxal, and dimethylglyoxal.[26,27,96] While in many cases our results do not allow for an unambiguous structural assignment of species that have clearly undergone some fragmentation, we can unambiguously distinguish oxidized and unoxidized species, and there is evidence that the most prevalent fragment ions are formed by breaking the weakest carbon−carbon or carbon−hydrogen bonds and that single O-atom or atomic ion addition takes place. Indeed, the fact that the mass spectra show distinct product distributions under different conditions, rather than a common, statistical distribution of ions ranging from carbon clusters to sequentially reduced and oxidized clusters, is evidence of a hierarchy of processes, with low-energy events such as electron attachment and ion−molecule association being the most important.

The evolution of species generated from the isoprene/O_2/UV gas mixture over minute time scales, mapped by measuring the mass spectra of discharge-generated anions probed by anion PE spectroscopy, revealed the production of both methylglyoxal and dimethylglyoxal. A limitation to using this method to more thoroughly explore the evolution of species from reactions initiated by ozonolysis of isoprene in the presence of O_2 is the evident destruction of a portion of the molecules. The destructiveness of the discharge limits our ability to make conclusions on the mechanism by which abundant smaller species, such as $HCOO^-$, are formed. Moreover, products with negative electron affinities will not be observed, while radical species formed in a discharge (i.e., reaction products that undergo −H loss in the discharge) will generally bind electrons, forming closed-shell anions.

Higher discharge voltages were necessary to produce ions from the isoprene/O_2/H_2 gas mixture, and the majority of anions beyond O_2^-, O_2^-·isoprene, and O_4^- observed predominantly resulted from the fragmentation of isoprene and the oxidation of those fragments. The structure of $C_4H_5^-$ (*m/z* 53) that was most consistent with the PE spectrum (**II**) results from breaking the longest and weakest carbon−carbon bond in isoprene (C2−CH_3). The formation of $C_5H_7^-$ *m/z* 67, then, results from loss of a hydrogen from the methyl group, which leads to a resonance-stabilized anion product. If the 53 and 67 amu radicals are formed first, they then can undergo O-atom or O^- atomic anion addition to form radical neutrals or closed-shell anions with *m/z* 69 and 83, respectively.

The differences between the mass spectra of anions generated from the isoprene/O_2/UV mixture and the isoprene/O_2/H_2 mixture are suggestive of the reactive species driving the chemistry in the expansion. For example, the relatively intense O_2^-·H_2O (*m/z* 50) signal observed in Figure 1c suggests water formation from coexpansion of O_2 and H_2 in the discharge, in addition to the hydroxyl radical or hydroxide anion. The moderately intense *m/z* 87 peak suggests reduction of the two double bonds predicted by calculations on the competitive isomers of *m/z* 83 (Figure 4e). The *m/z* 87 anion is comparatively low in abundance in the isoprene/O_2/UV-generated ions (Figure 1b), while species that have at least two O-atoms ($HCOO^-$, methylglyoxal, and dimethylglyoxal anions and their respective complex anions formed with O_2) and the species with *m/z* 76 may be due to the $[O_2\text{-}CO_2]^-$ complex anion.

The anion observed with *m/z* 69 is notably abundant under both isoprene/O_2/UV and isoprene/O_2/H_2 source conditions and is present, if not prominent, under the simple isoprene/O_2 conditions. The common spectroscopic feature observed in the

https://doi.org/10.1021/acs.jpca.1c08176
J. Phys. Chem. A 2021, 125, 10089−10102

anion PE spectra obtained under both isoprene/O_2/UV and isoprene/O_2/H_2 conditions points to a particularly stable $C_4H_5O^-$ molecular anion, which is interesting considering the absence of abundant precursor fragments that might intuitively react with atomic O or O^-. M/z 53 anions, or any "near neighbor" (that is, C_4H_y anions), are very low in abundance in all three gas mixtures. This suggests that m/z 69 would readily form from C_4H_y + O^-. It is also possible that a singlet oxygen ($^1\Delta_g$) + isoprene (68 amu) dioxetane formation reaction would cleave into two carbonyl-containing fragments[97] that could then undergo dissociative attachment resulting in the net loss of a proton from the methyl group, forming **II**, as shown in Scheme 1. Excited singlet states of O_2 are generated in the discharge, and this mechanism would (1) require no rearrangement of the 4-carbon backbone, (2) generate a stable conjugated molecular anion, and (3) account for the appearance of this ion under all three ion formation conditions, as O_2 is a common component in the gas mixtures.

Finally, several of the products observed in this study are species that have been predicted or observed in both ozonolysis of isoprene or hydrocarbon combustion. While the ion/neutral environments used in these experiments are very different from atmospheric conditions, the simplicity of this ion formation method and the vast variety of product forms suggest that this technique may be useful in the identification of potential products to aid in future combustion analyses. These studies would be further benefited by exploration of deuterated isoprene (C_5D_8) and deuterium reaction products.

CONCLUSIONS

A combined mass spectrometry and anion PE spectroscopic study on the oxidation of isoprene under several different oxidizing conditions was presented. Specifically, anions were generated via pulsed needled discharge through pulsed expansions of a UV-irradiated isoprene/O_2 mixture, which additionally produces O_3, and an isoprene/O_2/H_2 mixture, which generates $^{\bullet}$OH when passed through the discharge. The resulting mass spectra were compared to simple coexpansion of isoprene seeded in O_2. The identities of anions were investigated by analyzing their anion PE spectra and supported by computations. The mass spectra of ions generated under both conditions show the production of intact molecular ions and IMCs (e.g., O_2^-, O_4^-, O_2^-·isoprene) and singly deprotonated species (e.g., deprotonated isoprene, $C_5H_7^-$). In addition, smaller fragments and oxidized fragments are observed under both conditions, though relative abundances differ. From the UV-irradiated isoprene/O_2 gas mixture, additional intact molecular products of reactions initiated by ozonolysis of isoprene, methylglyoxal, and dimethylglyoxal were observed. Fragmentation and oxidation of isoprene are observed in both gas mixtures that are attributed to a series of alkyl- and alkenoxide anions. Overall, we observe the coexistence of intact molecules and IMCs, fragments and reaction products consistent with the lowest-energy isoprene fragmentation pathways, and fragments that suggest multistep destruction of isoprene and a hierarchy of ion production processes. Differences in the ion distributions formed under different conditions underscore this general method as a zero-order approach to identify potential reaction products that may be relevant to atmospheric or combustion chemistries (e.g., the evolution of ozonolysis reaction products in the presence of O_2), while ions that are common to all three conditions reported hint at other interesting chemical processes that lead to particularly stable species (e.g., $C_4H_5O^-$).

ASSOCIATED CONTENT

Supporting Information

The Supporting Information is available free of charge at https://pubs.acs.org/doi/10.1021/acs.jpca.1c08176.

Mass spectra of ions generated with the isoprene/O_2/UV gas mixture with different gas stagnation times; direct comparisons of several isoprene/O_2/UV and isoprene/O_2/H_2 product PE spectra of ions with coincident m/z; raw and reconstructed PE images of the isoprene/O_2/UV and isoprene/O_2/H_2 ions; comprehensive listings of calculated energies and structures; simulation parameters based on computed structures, vibrational frequencies, normal coordinates, and energies; and PE spectra of m/z 69 and m/z 83 obtained using 3.495 eV photon energy (PDF)

AUTHOR INFORMATION

Corresponding Author

Caroline Chick Jarrold − *Department of Chemistry, Indiana University, Bloomington, Indiana 47405, United States;* orcid.org/0000-0001-9725-4581; Email: cjarrold@indiana.edu

Authors

Marissa A. Dobulis − *Department of Chemistry, Indiana University, Bloomington, Indiana 47405, United States*

Michael C. Thompson − *Department of Chemistry, Indiana University, Bloomington, Indiana 47405, United States*

Complete contact information is available at: https://pubs.acs.org/10.1021/acs.jpca.1c08176

Notes

The authors declare no competing financial interest.

ACKNOWLEDGMENTS

The authors gratefully acknowledge support for this research from the National Science Foundation, Grant Nos. CHE-1664965 and CHE-2053889.

REFERENCES

(1) Bond, T. C.; Streets, D. G.; Yarber, K. F.; Nelson, S. M.; Woo, J.-H.; Klimont, Z. A Technology-Based Global Inventory of Black and Organic Carbon Emissions from Combustion *J. Geophys. Res.* 2004, *109*, D14203 DOI: 10.1029/2003JD003697.

(2) May, A. A.; Levin, E. J. T.; Hennigan, C. J.; Riipinen, I.; Lee, T.; Collett, J. L., Jr.; Jimenez, J. L.; Kreidenweis, S. M.; Robinson, A. L. Gas-Particle Partitioning of Primary Organic Aerosol Emissions: 3. Biomass Burning. *J. Geophys. Res.: Atmos.* **2013**, *118*, 11327−11338.

(3) Alfarra, M. R.; Prevot, A. S. H.; Szidat, S.; Sandradewi, J.; Weimer, S.; Lanz, V. A.; Schreiber, D.; Mohr, M.; Baltensperger, U. Identification of the Mass Spectral Signature of Organic Aerosols from Wood Burning Emissions. *Environ. Sci. Technol.* **2007**, *41*, 5770−5777.

(4) de Koning, H. W.; Smith, K. R.; Last, J. M. Biomass Fuel Combustion and Health. *Bull. World Health Organ* **1985**, *63*, 11−26.

(5) Lighty, J. S.; Veranth, J. M.; Sarofim, A. F. Combustion Aerosols: Factors Governing Their Size and Composition and Implications to Human Health. *J. Air Waste Manage.* **2000**, *50*, 1565−1618.

(6) Homann, K.-H. Fullerenes and Soot Formation—New Pathways to Large Particles in Flames. *Agnew. Chem., Int. Ed.* **1998**, *37*, 2434−2451.

(7) Frenklach, M. Reaction Mechanism of Soot Formation in Flames. *Phys. Chem. Chem. Phys.* **2002**, *4*, 2028−2037.
(8) Wang, H. Formation of Nascent Soot and Other Condensed-Phase Materials in Flames. *Proc. Combust. Inst.* **2011**, *33*, 41−67.
(9) Mansurov, Z. A. Soot Formation in Combustion Processes (Review). *Combust., Explos. Shock Waves* **2005**, *41*, 727−744.
(10) Ritcher, H.; Howard, J. B. Formation of Polycyclic Aromatic Hydrocarbons and Their Growth to Soot—A Review of Chemical Reaction Pathways. *Prog. Energy Combust. Sci.* **2000**, *26*, 565−608.
(11) Hansen, N.; Miller, J. A.; Klippenstein, S. J.; Westmoreland, P. R.; Kohs- Höinghaus, K. Exploring Formation Pathways of Aromatic Compounds in Laboratory-Based Models of Aliphatic Fuels. *Combust., Explos. Shock Waves* **2012**, *48*, 508−515.
(12) Comandini, A.; Brezinsky, K. Theoretical Study of the Formation of Naphthalene from the Radical/π-Bond Addition between Single-Ring Aromatic Hydrocarbons. *J. Phys. Chem. A* **2011**, *115*, 5547−5559.
(13) McEnally, C. S.; Pfefferle, L. D. Improving Sooting Tendency Measurements for Aromatic Hydrocarbons and Their Implications for Naphthalene Formation Pathways. *Combust. Flame* **2007**, *148*, 210−222.
(14) Moriarty, N. W.; Frenklach, M. *AB Initio* Study of Naphthalene Formation By Addition of Vinylacetylene to Phenyl. *Proc. Combust. Inst.* **2000**, *28*, 2563−2568.
(15) McCabe, M. N.; Hemberger, P.; Reusch, E.; Bodi, A.; Bouwman, J. Off the Beaten Path: Almost Clean Formation of Indene from the *ortho*-Benzene + Allyl Reaction. *J. Phys. Chem. Lett.* **2020**, *11*, 2859−2863.
(16) Liu, P.; Jin, H.; Chen, B.; Yang, J.; Li, Z.; Bennett, A.; Farooq, A.; Sarathy, S. M.; Roberts, W. L. Rapid Soot Inception via α-Alkynyl Substitution of Polycylcic Aromatic Hydrocarbons. *Fuel* **2021**, *295*, 120580.
(17) Adamson, B. D.; Skeen, S. A.; Ahmed, M.; Hansen, N. Detection of Aliphatically Bridged Multi-Core Polycyclic Aromatic Hydrocarbons in Sooting Flames with Atmospheric-Sampling High-Resolution Tandem Mass Spectrometry. *J. Phys. Chem. A* **2018**, *122*, 9338−9349.
(18) Baroncelli, M.; Mao, Q.; Galle, S.; Hansen, N.; Pitsch, H. Role of Ring-Enlargement Reactions in the Formation of Aromatic Hydrocarbons. *Phys. Chem. Chem. Phys.* **2020**, *22*, 4699−4714.
(19) Bouwman, J.; Hrodmarsson, H. R.; Ellison, G. B.; Bodi, A.; Hemberger, P. Five Birds with One Stone: Photoelectron Photoion Coincidence Unveils Rich Phthalide Pyrolysis Chemistry. *J. Phys. Chem. A* **2021**, *125*, 1738−1746.
(20) Hansen, N.; Kasper, T.; Klippenstein, S. J.; Westmoreland, P. R.; Law, M. E.; Taatjes, C. A.; Kohs- Höinghaus, K.; Wang, J.; Cool, T. A. Initial Steps of Aromatic Ring Formation in a Laminar Premixed Fuel-Rich Cyclopentene Flame. *J. Phys. Chem. A* **2007**, *111*, 4081−4092.
(21) Johansson, K. O.; Head-Gordon, M. P.; Schrader, P. E.; Wilson, K. R.; Michelsen, H. A. Resonance-Stabilized Hydrocarbon-Radical Chain Reactions May Explain Soot Inception and Growth. *Science* **2018**, *361*, 997−1000.
(22) Zhao, L.; Kaiser, R. I.; Lu, W.; Xu, B.; Ahmed, M.; Morozov, A. N.; Mebel, A. M.; Howlader, A. H.; Wnuk, S. F. Molecular Mass Growth through Ring Expansion in Polycyclic Aromatic Hydrocarbons via Radical-Radical Reactions. *Nat. Commun.* **2019**, *10*, No. 3689.
(23) McCabe, M. N.; Hemberger, P.; Reusch, E.; Bodi, A.; Bouwman, J. Off the Beaten Path: Almost Clean Formation of Indene from the *ortho*-Benzyne + Allyl Reaction. *J. Phys. Chem. Lett.* **2020**, *11*, 2859−2863.
(24) Porfiriev, D. P.; Azyazov, V. N.; Mebel, A. A. Conversion of Acenaphthalene to Phenalene via Methylation: A Theoretical Study. *Combust. Flame* **2020**, *213*, 302−313.
(25) Guenther, A. B.; Jiang, X.; Heald, C. L.; Sakulyanontvittaya, T.; Duhl, T.; Emmons, L. K.; Wang, X. The Model of Emissions of Gases and Aerosols from Nature Version 2.1 (MEGAN2.1): An Extended and Updated Framework for Modeling Biogenic Emissions. *Geosci. Model Dev.* **2012**, *5*, 1471−1492.
(26) Dobulis, M. A.; Thompson, M. C.; Patros, K. M.; Sommerfeld, T.; Jarrold, C. C. Emerging Nonvalence Anion States of [Isoprene-H·]·H2O Accessed via Detachment of OH^-·Isoprene. *J. Phys. Chem. A* **2020**, *124*, 2279−2287.
(27) Patros, K. M.; Mann, J. E.; Jarrold, C. C. Photoelectron Imaging Spectra of O_2^-•VOC and O_4^-•VOC Complexes. *J. Phys. Chem. A* **2016**, *120*, 7828−7838.
(28) Khaled, F.; Giri, B. R.; Liu, D.; Assaf, E.; Fittschen, C.; Farooq, A. Insights into the Reactions of Hydroxyl Radical with Diolefins from Atmospheric to Combustions Environments. *J. Phys. Chem. A* **2019**, *123*, 2261−2271.
(29) Atkinson, R.; Baulch, D. L.; Cox, R. A.; Crowley, J. N.; Hampson, R. F.; Hynes, R. G.; Jenkin, M. E.; Rossi, M. J.; Troe, J. Evaluated Kinetic and Photochemical Data for Atmospheric Chemistry: Volume II—Gas Phase Reactions of Organic Species. *Atmos. Chem. Phys.* **2006**, *6*, 3625−4055.
(30) Atkinson, R.; Arey, J. Gas-Phase Tropospheric Chemistry of Biogenic Volatile Organic Compounds: A Review. *Atmos. Environ.* **2003**, *37*, 197−219.
(31) Nguyen, T. B.; Tyndall, G. S.; Crounse, J. D.; Teng, A. P.; Bates, K. H.; Schwantes, R. H.; Coggon, M. M.; Zhang, L.; Feiner, P.; Miller, D. O.; et al. Atmospheric fates of Criegee Intermediates in the Ozonolysis of Isoprene. *Phys. Chem. Chem. Phys.* **2016**, *18*, 10241−10254.
(32) Wennberg, P. O.; Bates, K. H.; Crounse, J. D.; Dodson, L. G.; McVay, R. C.; Mertens, L. A.; Nguyen, T. B.; Praske, E.; Schwantes, R. H.; Smarte, M. D.; et al. Gas-Phase Reactions of Isoprene and Its Major Oxidation Products. *Chem. Rev.* **2018**, *118*, 3337−3390.
(33) Fiore, A. M.; Horowitz, L. W.; Purves, D. W.; Levy, H.; Evans, M. J.; Wang, Y.; Li, Q.; Yantosca, R. M. Evaluating the Contribution of Changes in Isoprene Emissions to Surface Ozone Trends over the Eastern United States *J. Geophys. Res.* 2005, *110*, D12303 DOI: 10.1029/2004JD005485.
(34) Douberly, G. E.; Ricks, A. M.; Ticknor, B. W.; McKee, W. C.; Schleyer, P. v. R.; Duncan, M. A. Infrared Photodissociation Spectroscopy of Protonated Acetylene and Its Clusters. *J. Phys. Chem. A* **2008**, *112*, 1897−1906.
(35) Freel, K.; Park, J.; Lin, M. C.; Heaven, M. C. Cavity Ring-Down Spectroscopy of the Phenyl Radical in a Pulsed Discharge Supersonic Jet Expansion. *Chem. Phys. Lett.* **2011**, *507*, 216−220.
(36) Ricks, A. M.; Douberly, G. E.; Schleyer, P. v. R.; Duncan, M. A. Infrared Spectroscopy of Protonated Ethylene: The Nature of Proton Binding in the Non-Classical Structure. *Chem. Phys. Lett.* **2009**, *480*, 17−20.
(37) Cazzoli, G.; Puzzarini, C. Observation of OD^- by Microwave Spectroscopy. *J. Chem. Phys* **2005**, *123*, 041101.
(38) Lattanzi, V.; Gottlieb, C. A.; Thaddeus, P.; Thorwirth, S.; McCarthy, M. C. The Rotational Spectrum of the NCO^- Anion. *Astrophys. J.* **2010**, *720*, 1717.
(39) Amano, T. Extended Negative Glow and "Hollow Anode" Discharges for Submillimeter-Wave Observation of CN^-, C_2H^-, and C_4H^-. *J. Chem. Phys.* **2008**, *129*, 244305.
(40) Lu, Y.-J.; Lehman, J. H.; Lineberger, W. C. A Versatile, Pulsed Anion Source Utilizing Plasma-Entrainment: Characterization and Applications. *J. Chem. Phys.* **2015**, *142*, 044201.
(41) Taylor, T. R.; Bise, R. T.; Asmis, K. R.; Neumark, D. M. The Singlet-Triplet Splitting of NCN. *Chem. Phys. Lett.* **1999**, *301*, 413−416.
(42) Lehman, J. H.; Lineberger, W. C. Photoelectron Spectroscopy of the Thiazate (NSO^-) and Thionitrite (SNO^-) Isomer Anions. *J. Chem. Phys.* **2017**, *147*, 013943.
(43) Shen, B. B.; Benitez, Y.; Lunny, K. G.; Continetti, R. E. Internal Energy Dependence of the Photodissociation Dynamics of O_3^- Using Cryogenic Photoelectron-Photofragment Coincidence Spectroscopy. *J. Chem. Phys.* **2017**, *147*, 094307.

(44) Chambers, D. M.; McLuckey, S. A.; Glish, G. L. Role of Gas Dynamics in Negative Ion Formation in an Atmospheric Sampling Glow Discharge Ionization Source. *Anal. Chem.* **1993**, *65*, 778−783.
(45) Grzesiak, J.; Vashishta, M.; Djuricani, P.; Stienkmeier, F.; Mudrich, M.; Dulitz, K.; Momose, T. Production of Rotationally Cold Methyl Radicals in Pulsed Supersonic Beams. *Rev. Sci. Instrum.* **2018**, *89*, 113103.
(46) Okumura, T.; Matsuda, S.; Satoh, Y.; Sakai, Y.; Tagashira, H. Decomposition of NO_2 in a Glow Discharge and Electron Impact Ionization and Attachment Coefficients in NO_2/Air Mixtures. *J. Phys. D: Appl. Phys.* **1994**, *27*, 801.
(47) Kaiser, R. I.; Hansen, N. An Aromatic Universe—A Physical Chemistry Perspective. *J. Phys. Chem. A* **2021**, *125*, 3826−3840.
(48) Snow, T. P.; Bierbaum, V. M. Ion Chemistry in the Interstellar Medium. *Annu. Rev. Anal. Chem.* **2008**, *1*, 229−259.
(49) Millar, T. J.; Walsh, C.; Field, T. A. Negative ions in Space. *Chem. Rev.* **2017**, *117*, 1765−1795.
(50) Mann, J. E.; Troyer, M. E.; Jarrold, C. C. Photoelectron Imaging and Photodissociation of Ozonide in $O_3^-\bullet(O_2)_n$ (n = 1-4) clusters. *J. Chem. Phys.* **2015**, *142*, 124305.
(51) Oliveira, A. M.; Lehman, J. H.; McCoy, A. B.; Lineberger, W. C. Photoelectron Spectroscopy of the Hydroxymethoxide Anion, $H_2C(OH)O^-$. *J. Chem. Phys.* **2016**, *145*, 124317.
(52) Duncan, M. A. Infrared Laser Spectroscopy of Mass-Selected Carbocations. *J. Phys. Chem. A* **2012**, *116*, 11477−11491.
(53) Posey, L. A.; Deluca, M. J.; Johnson, M. A. Demonstration of a Pulsed Photoelectron Spectrometer on Mass-Selected Negative Ion: O^-, $O2^-$, and $O4^-$. *Chem. Phys. Lett* **1986**, *131*, 170−174.
(54) Bakker, J. M. B. A Beam-Modulated Time-of-Flight Mass Spectrometer. I. Theoretical Considerations. *J. Phys. E: Sci. Instrum.* **1973**, *6*, 785−789.
(55) Bakker, J. M. B. A Beam-Modulated Time-of-Flight Mass Spectrometer. II. Experimental Work. *J. Phys. E: Sci. Instrum.* **1974**, *7*, 364−368.
(56) Eppink, A. T. J. B.; Parker, D. H. Velocity Map Imaging of Ions and Electrons Using Electrostatic Lenses: Application in Photoelectron and Photofragment Ion Imaging of Molecular Oxygen. *Rev. Sci. Instrum.* **1997**, *68*, 3477−3484.
(57) Chandler, D. W.; Houston, P. L. Two-Dimensional Imaging of State-Selected Photodissociation Products Detected by Multiphoton Ionization. *J. Chem. Phys.* **1987**, *87*, 1445.
(58) Doyle, M. B.; Abeyasera, C.; Suits, A. G. NuAcq 0.9: Native Megapixel Ion Imaging with Centroiding to 4 Mpix Using Inexpensive USB-2 Cameras. Available at http://faculty.missouri.edu/suitsa/NuAqc.html.
(59) Dribinski, V.; Ossadtchi, A.; Mandelshtam, V. A.; Reisler, H. Reconstruction of Abel-Transformable Images: The Gaussian Basis-Set Expansion Abel Transform Method. *Rev. Sci. Instrum.* **2002**, *73*, 2634−2642.
(60) Ervin, K. M.; Anusiewicz, I.; Skurski, P.; Simons, J.; Lineberger, W. C. The Only Stable State of O_2^- is the X $^2\Pi_g$ Ground State and It (Still!) Has an Adiabatic Electron Detachment Energy of 0.45 eV. *J. Phys. Chem. A* **2003**, *107*, 8521−8529.
(61) Garcia, G. A.; Nahon, L.; Powis, N. Two-Dimensional Charged Particle Image Inversion Using a Polar Basis Function Expansion. *Rev. Sci. Instrum.* **2004**, *75*, 4989.
(62) Frisch, M. J.; Trucks, G. W.; Schlegel, H. B.; Scuseria, G. E.; Robb, M. A.; Cheeseman, J. R.; Scalmani, G.; Barone, V.; Petersson, G. A.; Nakatsuji, H. et al. *Gaussian 16*, Rev. C.01; Gaussian, Inc.: Wallingford, CT, USA, 2016.
(63) Yanai, T.; Tew, D. P.; Handy, N. C. A New Hybrid Exchange-Correlation Functional Using the Coulomb Attenuating Method (CAM-B3LYP). *Chem. Phys. Lett.* **2004**, *393*, 51−57.
(64) Schäfer, A.; Huber, C.; Ahlrichs, R. Fully Optimized Contracted Gaussian Basis Sets of Triple Zeta Valence Quality for Atoms Li to Kr. *J. Chem. Phys.* **1994**, *100*, 5829.
(65) Hunziker, H. E.; Kneppe, H.; Wendt, H. R. Photochemical Modulation Spectroscopy of Oxygen with Olefins. *J. Photochem.* **1981**, *17*, 377−387.
(66) Yacovitch, T. I.; Garand, E.; Neumark, D. M. Slow Photoelectron Velocity-Map Imaging Spectroscopy of the Vinoxide Anion. *J. Chem. Phys.* **2009**, *130*, 244309.
(67) Alconcel, L. S.; Deyerl, H.-J.; Zengin, V.; Continetti, R. E. Structure and Energetics of Vinoxide and the X(^{2}A″) and the X(^{2}A′) Vinoxy Radicals. *J. Phys. Chem. A* **1999**, *103*, 9190−9194.
(68) Krylov, A. I. Equation-of-Motion Coupled-Cluster Methods for Open-Shell and Electronically Excited Species: The Hitchhiker's Guide to Fock Space. *Annu. Rev. Phys. Chem.* **2008**, *59*, 433−462.
(69) Schaugaard, R. N.; Topolski, J. E.; Ray, M.; Raghavachari, K.; Jarrold, C. C. Insight into Ethylene Interactions with Molybdenum Suboxide Cluster Anions from Photoelectron Spectra of Chemifragments. *J. Chem. Phys.* **2018**, *148*, 054308.
(70) Dauletyarov, Y.; Dixon, A. R.; Wallace, A. A.; Sanov, A. Electron Affinity and Excited States of Methylglyoxal. *J. Chem. Phys.* **2017**, *147*, 013934.
(71) Dauletyarov, Y.; Wallace, A. A.; Blackstone, C. C.; Sanov, A. Photoelectron Spectroscopy of Biacetyl and Its Cluster Anions. *J. Phys. Chem. A* **2019**, *123*, 4158−4167.
(72) Yu, J.; Jeffries, H. E.; Le Lacheur, R. M. Identifying Airborne Carbonyl Compounds in Isoprene Atmospheric Photooxidation Products by Their PFBHA Oximes Using Gas Chromatography/Ion Trap Mass Spectrometry. *Environ. Sci. Technol.* **1995**, *29*, 1923−1932.
(73) Lee, S. H.; Kim, N.; Kim, T.-R.; Shin, S.; Kim, S. K. Electron Attachment to the $(O_2...CO_2)$ van der Waals Complex Results in a Monomeric Anion $(O_2\text{-}CO_2)^-$, a Possible Form of CO_4^-. *J. Phys. Chem. A* **2021**, *125*, 5794−5799.
(74) Dobulis, M. A.; McGee, C. J.; Sommerfeld, T.; Jarrold, C. C. A Autodetachment over Broad Photon Energy Ranges in the Anion Photoelectron Spectra of $[O_2\text{-}M]^-$ (M = Glyoxal, Methylglyoxal, Biacetyl) Complex Anions. *J. Phys. Chem. A* **2021**, *125*, 9128−9142.
(75) Ellison, G. B.; Engelking, P. C.; Lineberger, W. C. Photoelectron Spectroscopy of Alkoxide and Enolate Negative Ions. *J. Phys. Chem. A* **1982**, *86*, 4873−4878.
(76) Poad, B.L.J.; Ray, A. W.; Continetti, R. E. Dissociative Photodetachment of the Ethoxide Anion and Stability of the Ethoxy Radical $CH_3CH_2O\cdot$. *J. Phys. Chem. A* **2013**, *117*, 12035−12041.
(77) Kim, E. H.; Bradforth, S. E.; Arnold, D. W.; Metz, R. B.; Neumark, D. M. Study of HCO_2 and DCO_2 by Negative Ion Photoelectron Spectroscopy. *J. Chem. Phys.* **1995**, *103*, 7801.
(78) Johnson, C. J.; Harding, M. E.; Poad, B. L.; Stanton, J. F.; Continetti, R. E. Electron Affinities, Well Depths, and Vibrational Spectroscopy of *cis*- and *trans*-HOCO. *J. Am. Chem. Soc.* **2011**, *133*, 19606−19609.
(79) Patros, K. M.; Mann, J. E.; Dobulis, M. A.; Thompson, M. C.; Jarrold, C. C. Probing Alkenoxy Radical Electronic Structure Using Anion PEI Spectroscopy. *J. Chem. Phys.* **2019**, *150*, 034302.
(80) Ramond, T. M.; Davico, G. E.; Schwartz, R. L.; Lineberger, W. C. Vibronic Structure of Alkoxy Radicals via Photoelectron Spectroscopy. *J. Chem. Phys.* **2000**, *112*, 1158.
(81) Alconcel, L. S.; Deyerl, H.-J.; DeClue, M.; Continetti, R. E. Dissociation Dynamics and Stability of Cyclic Alkoxy Radicals and Alkoxide Anions. *J. Am. Chem. Soc.* **2001**, *123*, 3125−3132.
(82) Stokes, S. T.; Bartmess, J. E.; Buonaugurio, A.; Wang, Y.; Eustis, S. N.; Bowen, K. H. Anion Photoelectron Spectroscopy of the Linear $C_nH_{n+1}O^-$ (n=1-9) alkoxides. *Chem. Phys. Lett.* **2019**, *732*, 136638.
(83) Wang, X.-B.; Woo, H.-K.; Wang, L.-S.; Minofar, B.; Jungwirth, P. Determination of the Electron Affinity of the Acetyloxyl Radical (CH_3COO) by Low-Temperature Anion Photoelectron Spectroscopy and ab Initio Calculations. *J. Phys. Chem. A* **2006**, *110*, 5047−5050.
(84) Oliveira, A. M.; Lu, Y.-J.; Lehman, J. H.; Changala, P. B.; Baraban, J. H.; Stanton, J. F.; Lineberger, W. C. Photoelectron Spectroscopy of the Methide Anion: Electron Affinities of $\bullet CH_3$ and $\bullet CD_3$ and Inversion Splittings of CH_3^- and CD_3^-. *J. Am. Chem. Soc.* **2015**, *137*, 12939−12945.
(85) Gunion, R. F.; Lineberger, W. C. Ultraviolet Photoelectron Spectroscopy of the *tert*-Butylvinylidene Anion. *J. Phys. Chem. B* **1996**, *100*, 4395−4399.

https://doi.org/10.1021/acs.jpca.1c08176
J. Phys. Chem. A 2021, 125, 10089−10102

(86) Wenthold, P. G.; Polak, M. L.; Lineberger, W. C. Photoelectron Spectroscopy of the Allyl and 2-Methylallyl Anions. *J. Phys. Chem. C* **1996**, *100*, 6920−6929.
(87) Oakes, J. M.; Ellison, G. B. Photoelectron Spectroscopy of the Allenyl Ion CH_2=C=CH^-. *J. Am. Chem. Soc.* **1983**, *105*, 2969−2975.
(88) Robinson, M. S.; Polak, M. L.; Bierbaum, V. M.; DePuy, C. H.; Lineberger, W. C. Experimental Studies of Allene, Methylacetylene, and the Propargyl Radical: Bond Dissociation Energies, Gas-Phase Acidities, and Ion-Molecule Chemistry. *J. Am. Chem. Soc.* **1995**, *117*, 6766−6778.
(89) Parker, C. L.; Cooksy, A. L. Ab Initio Study of the 1,3-butadienyl Radical Isomers. *J. Phys. Chem. A* **1998**, *102*, 6186−6190.
(90) Parker, C. L.; Cooksy, A. L. Ab Initio Study of the Most Stable C_4H_5 Isomers. *J. Phys. Chem. A* **1999**, *103*, 2160−2169.
(91) Vogelhuber, K. M.; Wren, S. W.; Sheps, L.; Lineberger, W. C. The C−H Bond Dissociation Energy of Furan: Photoelectron Spectroscopy of the Furanide Anion. *J. Chem. Phys.* **2011**, *134*, 064302.
(92) Culberson, L. M.; Sanov, A. Electronic States of Thiophenyl and Furanyl Radicals and Dissociation Energy of Thiophene via Photoelectron Imaging of Negative Ions. *J. Chem. Phys.* **2011**, *134*, 204306.
(93) Reilly, N. J.; da Silva, G.; Wilcox, C. M.; Zijun, G.; Kokkin, D. L.; Troy, T. P.; Nauta, K.; Kable, S. H.; McCarthy, M. C.; Schmidt, T. W. Interconversion of Methyltropyl and Xylyl Radicals: A Pathway Unavailable to the Benzyl-Tropyl Rearrangement. *J. Phys. Chem. A* **2018**, *122*, 1261−1269.
(94) Reilly, N. J.; Nakajima, M.; Troy, T. P.; Chalyavi, N.; Duncan, K. A.; Nauta, K.; Kable, S. H.; Schmidt, T. W. Spectroscopic Identification of the Resonance-Stabilized *cis*- and *trans*-1-Vinyl-propargyl Radicals. *J. Am. Chem. Soc.* **2009**, *131*, 13423−13429.
(95) Reilly, N. J.; Kokkin, D. L.; Ward, M. L.; Flores, J.; Ross, S. D.; McCaslin, L. M.; Stanton, J. F. Gas-Phase Optical Detection of 3-Ethynylcyclopentenyl: A Resonance-Stabilized C_7H_7 Radical with an Embedded 1-Vinylpropargyl Chromophore. *J. Am. Chem. Soc.* **2020**, *142*, 10400−10411.
(96) Patros, K. M.; Mann, J. E.; Jarrold, C. C. O_2^-• [Polar VOC] Complexes: H-Bonding versus Charge-Dipole Interactions, and the Noninnocence of Formaldehyde. *J. Phys. Chem. A* **2017**, *121*, 5459−5467.
(97) Frimer, A. A. The Reaction of Singlet Oxygen with Olefins: The Question of Mechanism. *Chem. Rev.* **1979**, *79*, 359−387.

https://doi.org/10.1021/acs.jpca.1c08176
J. Phys. Chem. A 2021, 125, 10089−10102